ELSEVIER

Contents lists available at ScienceDirect

Journal of Inorganic Biochemistry

journal homepage: www.elsevier.com/locate/jinorgbio





In vitro anti-Leishmania activity of new isomeric cobalt(*II*)complexes and *in silico* insights: Mitochondria impairment and apoptosis-like cell death of the parasite[†]

Samuel M. Rocha ^a, Adolfo Horn Jr. ^a, Aline R. de M. L. Terra ^b, Lara M. Rezende ^b, Felipe F. Moreira ^b, Renato A. DaMatta ^b, Fernando R. Xavier ^c, Rodrigo Cervo ^d, Roberta Cargnelutti ^d, Sreerag N. Moorkkannur ^e, Graysen Owenby ^e, Rajeev Prabhakar ^e, Sérgio H. Seabra ^{b,*}, Christiane Fernandes ^{a,*}

- ^a Departamento de Química, Universidade Federal de Santa Catarina, 88040-900 Florianópolis, SC, Brazil
- b Laboratório de Biologia Celular e Tecidual, Universidade Estadual do Norte Fluminense Darcy Ribeiro, 28013-602 Campos dos Goytacazes, RJ, Brazil
- ^c Departamento de Química, Universidade do Estado de Santa Catarina, 89219-710 Joinville, SC, Brazil
- ^d Departamento de Química, Universidade Federal de Santa Maria, 97105-900 Santa Maria, RS, Brazil
- ^e Department of Chemistry, University of Miami, Coral Gables, FL 33146, USA

ARTICLE INFO

Keywords: Cobalt(II) complexes X-ray Leishmania amazonensis Leishmanicidal activity Molecular docking Apontotic mechanism

ABSTRACT

The synthesis, physico-chemical characterization and in vitro antiproliferative activity against the promastigote form of Leishmania amazonensis of two new cobalt(II) coordination compounds (i.e. [Co(HL1)Cl₂]0.4,2H₂O (1) and $[Co(HL2)(Cl)(CH_3OH)](ClO_4).2H_2O$ (2)) are reported, where $HL1 = 4-\{3-[bis(pyridin-2-ylmethyl)amino]-2-ylmethyl)$ hydroxypropoxy}-2H-chromen-2-one and HL2 = 7-{3-[bis(pyridin-2-ylmethyl)amino]-2-hydroxypropoxy}-2Hchromen-2-one. X-ray diffraction studies were performed for complex (2) and the structure of complex (1) was built through Density Functional Theory (DFT) calculations. Complex (1) presented no cytotoxicity to LLC-MK2, but complex (2) was toxic. IC₅₀ against promastigotes of L. amazonensis for complex (1) were 4.90 (24 h), 3.50 (48 h) and 3. 80 μ mol L⁻¹ (72 h), and for complex (2) were 2.09, 4.20 and 2.80 μ mol L⁻¹, respectively. Due to the high toxicity presented by complex (2) against LLC-MK2 host cells, mechanistic studies, to shed light on the probable mode of leishmanicidal activity, were carried out only for the non-cytotoxic complex. Complex (1) was able to elevate mitochondrial membrane potential of the parasites after treatment. Transmission electron microscopy revealed typical apoptotic condensation of chromatin, altered kinetoplast and mitochondria structures, suggesting that apoptosis-like cell death of the protozoa is probably mediated by an apoptotic mechanism associated with mitochondrial dysfunction (intrinsic pathway). Molecular docking studies with complex (1) upon protein tyrosine phosphatase (LmPRL-1) suggests a plausible positive complex anchoring mainly by hydrophobic and hydrogen bond forces close to the enzyme's catalytic site. These promising results for complex 1 will prompt future investigations against amastigote form of L. amazonensis.

1. Introduction

Leishmaniasis consists of a wide spectrum of diseases caused by >20 different species of obligate intracellular protozoa belonging to the genus *Leishmania*, which are transmitted by the bite of infected female sand flies to mammalian hosts [1,2]. This disease is considered by the World Health Organization as an important public health problem, as

well as a neglected tropical disease. An estimated of 1.5–2 million new human cases of leishmaniasis per year are reported from nearly 100 endemic countries, including Asia, Africa, the Americas and the Mediterranean region [3].

Parasites belonging to the *Leishmania* genus have a complex life cycle that involves both vertebrate and invertebrate hosts. Two stages of development are found: (i) promastigote, proliferative form found in the

E-mail addresses: seabrash@uenf.br (S.H. Seabra), christiane.horn@ufsc.br (C. Fernandes).

^{*} Corresponding authors.

lumen of the intestine of the phlebotomine sand flies and (ii) amastigote, proliferative form found in various types of mammalian host cells [4], which can be hematopoietic or not, such as keratinocytes, Langerhans cells, neutrophils, macrophages and fibroblasts [5–8].

Leishmaniasis is a poverty-related disease with two main clinical forms: cutaneous (CL) and visceral leishmaniasis (VL) [3]. CL affects the skin, while VL affects the internal organs of the infected patients. VL is fatal in 95% of the cases if left untreated [9]. CL is caused by *L. major* and *L. tropica* in the Middle East and Central Asia, and *L. braziliensis* and *L. mexicana* complex in the Americas. Mucocutaneous leishmaniasis (MCL) is a serious and chronic infection [10]. In Brazil, *L. amazonensis* is one of the species responsible for the cutaneous form of the disease; in some individuals the immune system cannot fight the parasite, leading to clinical manifestations of diffuse cutaneous leishmaniasis (DCL) [1]. DCL was first reported in the Brazilian Amazon, in the state of Pará by Silva [11], who described the first clinical findings on a rare form of CL, highlighting the nature of keloid lesions on the skin and lesions in the bone tissue of the extremities (hands and feet).

Clinical features depend on the species of *Leishmania* and the immune response of the host. The mechanisms through which the parasite resists killing within the toxic environment of the phagolysosome remain incompletely defined. This is an increasing problem where HIV-infected individuals live in *Leishmania* endemic areas. Leishmaniasis is controlled through cell-mediated immune defenses [12], and it has been shown, in murine systems, that IFN- γ synergizes with TNF- α , inducing the expression of nitric oxide synthase to produce nitric oxide, killing the intracellular parasites [13].

Currently, the pentavalent antimonial compound, Glucantime® (meglumine antimoniate), and Amphotericin B are used in the treatment of leishmaniasis as first and second line drugs, respectively, being applied intramuscularly or intravenously. Further than their high cost, both are not very efficient because they often cause side effects, such as arthralgia, myalgia, nausea, tachycardia, fever and vomiting [14–16]. Given the scenario, there is an imminent need to develop new drugs.

Some studies have already shown that coordination compounds can be an alternative for pharmacological control of tropical parasitic diseases. In 2009, Gambino and co-workers have reported the antiparasitic activity against Kinetoplastids *Leishmania spp.* and *Trypanosoma cruzi* of a dinuclear gold(I) complex (IC50 of 1 μ mol L⁻¹). This complex was obtained employing the bioactive co-ligand pyridine-2-thiol N oxide (mpo), an effective NADH fumarate reductase inhibitor of *T. cruzi* epimastigotes. This gold(I) complex presents a potent leishmanicidal effect against promastigotes of L. *mexicana* while on L. *braziliensis* only a leishmanistatic effect was reported. The coordination of gold(I) to the bioactive ligand mpo improved the antiproliferative effect against both *Leishmania* species and *T. cruzi*, which was associated to the inhibition of NADH fumarate reductase (absent in mammalian cells) [17].

In 2019, Yoneyama and co-workers reported that the complex *cis*-[Ru(II)(η_2 O₂CC₇H₇O₂)(dppm)₂]PF₆ (hmxbato) and its precursor *cis*-[Ru (II)Cl₂(dppm)₂], where dppm is the ligand bis(diphenylphosphino) methane, promoted apoptosis-like death of L. *amazonensis* promastigotes which is related to alterations in parasite mitochondria, rise in ROS and increase in the formation of autophagic vacuoles in the parasite after 24 h of treatment [18].

Our group has been developing coordination compounds, containing the first row transition metal ions (Cu(II), Zn(II) and Fe(III)), as potential antiparasitary agents [19–23]. In 2017, we reported anti-*Toxoplasma* activity and ultrastructural analyzes of two Cu(II) complexes [21]. Both complexes irreversibly control the growth of the parasite *T. gondii in vitro*, resulting in IC₅₀ values of 3.57 and 0.78 μ mol L⁻¹, after 48 h of treatment. It was observed that these compounds induce the conversion of part of the parasites from the tachyzoite form to bradyzoite, with their subsequent death. In 2021 we reported the antichagasic activity of two isomeric Fe(III) complexes against *T. cruzi* epimastigotes at concentrations in the nanomolar range (IC₅₀ = 97–122 nmol L⁻¹), showing low cytotoxicity to the host cells LLC-MK2, resulting in a high selectivity

index (106 and 178, respectively). Treatment with both complexes, at nanomolar concentrations, generated important changes in mitochondria and reservosome of the parasite, which are essential organelles for their survival [22]. Recently, we reported the anti-toxoplasma activity and DFT studies of water-soluble complexes (Fe, Cu, Zn) containing the ligand N-2[(pyridine-2-ylmethyl)amino)ethanol. Among all compounds investigated, the Fe(III) complex [Fe(HL1)Cl₃] showed the best reduction in the infection index, promoting the death of the parasite [23].

In 2020, Eifler-Lima and co-workers demonstrated several examples of coumarins with remarkable potential against different species of Leishmania [24]. Recents reports indicate that the physicochemical and biological properties of coumarins might be enhanced by combining with metal ions, offering new possibilities in the development of new coordination compounds with specific and new modes of action [25–27]. In 2021, Kornicka and co-workers reported that the incorporation of a metal ion into coumarin derivatives can increase the activity of such complexes compared to coumarin-based ligands [27]. However, the leishmanicidal activity of metallic complexes containing coumarin ligands are rare in the literature, pointed out the importance of the development of coordination compounds containing coumarin-based ligands.

Considering that it has already been demonstrated that coordination compounds can be used as a good antiparasitic agents, and motivated by our previous results against *T. gondii* and *T. cruzi*, the aim of this work was to evaluate the leishmanicidal effect of two new isomeric Co(II) complexes *in vitro*. The study was carried out against the extracellular form (promastigote) of L. *amazonensis*. In addition, to investigate the cytotoxicity in a model host cells (LLC-MK2), as well as the effect of the isomerism of the ligand on leishmanicidal activity of these new Co(II) complexes containing a coumarin pendant unit. An *in silico* docking study between the most active complex and the protein tyrosine phosphatase from L. *major* (LmPRL-1) [28], as a possible biochemical target, was also performed.

2. Experimental

2.1. Materials and methods

The ligand and their respective complexes were synthesized using commercial grade reagents. UV-Vis, and ESI-(+)-MS investigations were carried out employing spectroscopic, HPLC or MS grade solvents. All chemicals and reagents were purchased from Sigma-Aldrich and used as such. ¹H and ¹³C NMR spectra were recorded with Bruker AVANCE DRX 400 MHz spectrometer. Chemical shifts (δ) are given in ppm, and the spectra were recorded in deuterated solvents, as indicated. TMS (0 ppm) was employed as standard. The elemental analysis (CHN) for the complexes was performed with a Perkin Elmer 2400 CHN analyzer. Infrared spectra were recorded with a Shimadzu FT-IR 8300 spectrophotometer. The solid samples were prepared in a KBr pellet and the spectra were recorded over the frequency range of 400–4000 cm⁻¹. UV–Vis spectra of the complexes were recorded in acetonitrile, in a UV-Vis Varian, Cary 50 Bio. The determination of melting points was made in the Microquimica MQAPF - 307 apparatus. Full scan mass spectra (MS mode) were obtained on an Electrospray Ionization (ESI-MS) Amazon X Ion Trap MS instrument (Bruker Daltonics, Germany), in positive mode, ion-source voltage of 4500 V, flow Injection or flow rate of 180 μL/h, nebulizing gas (0.4 bar) and dry gas (4 L min⁻¹), ion-source temperature 180 and 200 °C and the scan range was m/z 100–2000. The electrical conductivity of a 1×10^{-3} mol dm⁻³ solution of each complex was measured with a MS Tecnopon mCA-150 apparatus. Single-crystal X-ray diffraction data were carried out with a Bruker D8 Venture diffractometer equipped with a Photon 100 detector, Incoatec microfocus Montel optic X-ray tube with Ag-K α radiation ($\lambda=0.56086$ Å). The structure was solved and refined with the SHELX program package [29,30]. Non-hydrogen atoms were refined anisotropically. The molecular structure was drawn with Diamond program (version 4.6.0) [31]. The crystallographic

information file (CIF) for the complex **(2)** was deposited at the Cambridge Crystallographic Data Centre (CCDC) under identification number 2177601. These data can be obtained free of charge *via* http://www.ccdc.cam.ac.uk/conts/retrieving.html (or from the Cambridge Crystallographic Data Centre, 12, Union Road, Cambridge CB2 1EZ, UK; fax: +441,223 336,033). Crystal data and more details of the data collection and refinement of the complex **(2)** are provided in supporting information material (Table 3S).

2.2. Synthesis

2.2.1. Synthesis of the ligands HL1 and HL2

Ligand HL1 was prepared by the reaction between bis-(pyridin-2ylmethyl)amine (BMPA) [32] (0.02 mol, 4.00 g) and 4-(oxiran-2-ylmethoxy)-chromen-2-one (0.02 mol, 4.36 g), in ethanol (Scheme 1). The mixture was stirred for 14 days at 50 °C, which was follow by TLC, using methanol:ethyl acetate (9:1) as eluent. Subsequently, the solvent was removed under reduced pressure and the product was diluted with 50 mL of dichloromethane. The compound was washed with brine, dried over anhydrous MgSO₄, filtered and concentrated under reduced pressure. A brown oil was obtained. Yield: 6 g (72%). IR (cm⁻¹): ν (OH), 3200–3400; $\nu(CH_{ar-al})$, 2800–3200; $\nu(C=O)$, 1733; $\nu(C=C)$, 1613; ν (C=C_{ar}), 1600–1450; ν (C—O), 1280 and δ (C-H_{piridine ring}), 769. 1 H NMR (400 MHz, CDCl₃) δ /ppm: 2.83–2.89 (m, 1H), 3.88–4.03 (m, 6H), 4.17-4.23 (m, 1H), 4.20-4.33 (m, 1H), 5.55-5.70 (m, 1H), 7.08-7.22 (m, 2H), 7.11-7.23 (m, 2H), 7.30-7.34 (m, 2H), 7.40-7.47 (m, 1H), 7.50-7.60 (m, 2H), 7.67-7.78 (m, 1H) and 8.43-8.48 (dd, 2H). 13 C NMR (400 MHz, CDCl₃) δ /ppm: 54.10, 60.49, 68.81, 71.05, 90.48, 115.53, 116.70, 122.36, 122.52, 123.34, 123.96, 132.54, 136.85, 149.13, 153.25, 158.68, 163.06 and 165.61. Fig. 1S-3S present the ¹H NMR, COSY and HSQC spectra for HL1. Assignments were made according to 2D NMR data (Table 1S).

Ligand HL2 was prepared by the reaction between bis-(pyridin-2-ylmethyl)amine (BMPA) [32] (0.02 mol, 4.00 g) and 7-(oxiran-2-methoxy)-chromen-2-one (0.02 mol, 4.36 g), in ethanol (Scheme 1). The mixture was stirred for 14 days at 50 °C, which was follow by TLC, using methanol:ethyl acetate (9:1) as eluent. Subsequently, the solvent was removed under reduced pressure and the product was diluted with 50 cm³ of dichloromethane. The compound was washed with brine, dried over anhydrous MgSO₄, filtered and concentrated under reduced pressure. A brown oil was obtained. Yield: 6.1 g (79%). IR (cm $^{-1}$): ν (OH), 3200–3400; ν (CH_{ar-al}), 2800–3200; ν (C=O), 1733; ν (C=C), 1613; ν (C=C_{ar}), 1600–1450; ν (C—O), 1280; δ (CH_{piridine ring}), 769. 1 H NMR (400 MHz, CDCl₃) δ /ppm: 2.84–3.04 (m, 2H), 3.85–4.02 (m, 4H), 4.15 (d, 2H), 4.20 (m, 1H), 6.22 (m, 1H), 6.75–6.88 (m, 2H), 7.13–7.20 (m,

Scheme 1. Scheme of synthesis for ligands HL1 and HL2.

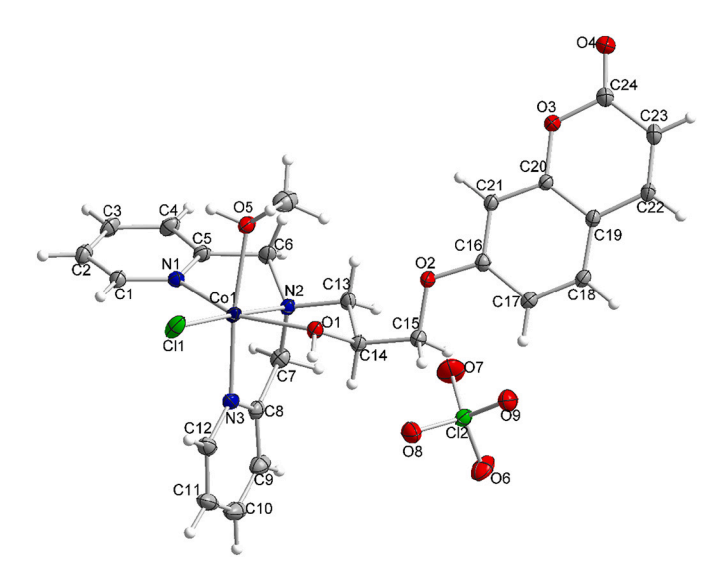


Fig. 1. Thermal ellipsoid plot at the 50% probability level for the complex **(2)**, obtained by X-ray crystallography.

Table 1Selected bond lengths (Å) and angles (°) for complex **(2)**.

| Bond lengths | | Angles | |
|---------------|-------------|---------------------|-----------|
| Co (1)–N (1) | 2.0910(19) | N (1)-Co (1)-O (1) | 155.44(7) |
| Co (1)-O (1) | 2.1196 (17) | N (1)-Co (1)-N (3) | 97.64(7) |
| Co (1)-N (3) | 2.125(2) | O (1)-Co (1)-N (3) | 90.63(7) |
| Co (1)-O (5) | 2.1642 (18) | N (1)-Co (1)-O (5) | 81.97(7) |
| Co (1)-N (2) | 2.169(2) | O (1)-Co (1)-O (5) | 86.24(7) |
| Co (1)-Cl (1) | 2.3511(11) | N (3)-Co (1)-O (5) | 170.84(7) |
| | | N (1)-Co (1)-N (2) | 78.32(7) |
| | | O (1)-Co (1)-N (2) | 80.46(7) |
| | | N (3)-Co (1)-N (2) | 79.88(8) |
| | | O (5)-Co (1)-N (2) | 91.10(7) |
| | | N (1)-Co (1)-Cl (1) | 103.11(6) |
| | | O (1)-Co (1)-Cl (1) | 98.50(5) |
| | | N (3)-Co (1)-Cl (1) | 98.18(6) |
| | | O (5)-Co (1)-Cl (1) | 90.81(6) |
| | | N (2)-Co (1)-Cl (1) | 177.76(5) |

2H), 7.25–7.40 (m, 3H), 7.55–7.69 (m, 3H) and 8.50–8.57 (dd, 2H). 13 C NMR (400 MHz, CDCl₃) δ /ppm: 57.95, 60.43, 67.68, 69.40, 101.56, 112.63, 112.94, 113.05, 121.94, 123.17, 128.70, 136.72, 143.47, 148.95, 155.74, 158.90, 161.28 and 162.07. Fig. 4S-6S present the 1 H NMR, COSY and HSQC spectra for HL2. The assignments were made according to 2D NMR data for HL2 (Table 2S).

2.2.2. Synthesis of $[Co(HL1)Cl_2]$.4,2 H_2O (1) and $[Co(HL2)(Cl)(CH_3OH)](ClO_4)$.2 H_2O (2)

The cited compounds (Scheme 2) were prepared reacting the ligands HL1 (1 mmol, 417 mg) or HL2 (1 mmol, 417 mg) and $[Co(H_2O)_6]Cl_2$ (1 mmol, 238 mg), in methanol, with constant stirring at 60 °C for 2 h. Thereafter, a green solid was obtained immediately after the reaction with HL1 and 1 mmol (106 mg) of LiClO₄ was only added to the solution containing the ligand HL2, resulting in a light purple solution. After allowing the solution to stand for a few days, light purple crystals, suitable for crystallographic analysis, were collected for complex (2), washed with cold propan-2-ol and dried in a desiccator. Complex (1) was obtained as a green solid and unfortunately no good quality crystals were obtained, after several recrystallizations. For complex (1): Yield: 0.29 g (47%). m.p. 200 °C. IR (cm⁻¹): ν (OH), 3510–3200; ν (CH), 3100–3000; ν (CH₂), 3000–2800(s); ν (C=O), 1704; ν (C=C_{ar}), 1600–1450; ν (C=O), 1239; δ (CH_{piridine ring}), 769. (Fig. 7S presents the IR spectrum for the ligand HL1 and for complex (1)). Anal. Calcd for [Co

Scheme 2. Synthesis of complexes (1) and (2).

 $(HL1)Cl_2]0.4.2H_2O$ (1) $(CoC_{24}H_{31.4}Cl_2N_3O_{8.2}, MW = 622.98 g mol^{-1})$: C, 46.27; H, 5.08; N, 6.74. Found: C, 46.06; H, 4.71; N, 6.86%. UV-Vis λ (nm) data (ϵ , L mol⁻¹ cm⁻¹): 588 (660), 629 (541), 658 (609) and 684 (647). (Fig. 17S) Ω (CH₃CN) = 17.44 μ S cm⁻¹ (non electrolyte). ESI-(+)-MS in acetonitrile: $[M]^+ = 511$: $[Co(HL1)Cl]^+$ (Fig. 4, Fig. 9S and 10S). For complex (2): Yield: 0.41 g (64%). m.p. 173 °C. IR (cm⁻¹): ν (OH), 3450–3200; ν (CH_{ar-al}), 3100–2800; ν (C=O), 1701; ν (C=C_{ar}), 1600–1450; ν (C—O), 1230; ν (ClO₄), 1085, 1116 and 1156; δ (CH_{piridine} ring), 769. (Fig. 8S presents the IR spectrum for the ligand HL2 and for complex (2)). Anal. Calcd for [Co(HL2)(OHCH3)Cl]ClO4.2H2O (2) $(CoC_{25}H_{31}Cl_2N_3O_{11}, MW = 679.34 \text{ g mol}^{-1})$: C, 44.24; H, 4.57; N, 6.19. Found: C, 44.30; H, 4.24; N, 6.32%. UV–Vis λ (nm) data (ϵ , dm³ mol⁻¹ cm⁻¹): 486 (87), 508 (93), 603 (94), 623 (87) and 780 (21) (Fig. 3). $\Omega_{CH3CN}=133.7~\mu S~cm^{-1}$ (1:1 electrolyte). ESI-(+)-MS in acetonitrile: $[M]^+ = 511$: $[Co(HL2)Cl]^+$ (Fig. 11-16S). X-ray diffraction data indicates the absent of water molecules as hydration solvent. Elemental analysis indicates the presence of two water molecules as hydration solvent. The crystals were kept in desiccator until analysis and this justify this difference.

2.3. Anti-Leishmania activity and host cell viability

2.3.1. Culture of Leishmania amazonensis

The promastigote form of L. *amazonensis* (Josefa strain), obtained from the differentiation of amastigotes isolated from lesions in Balb/C mice, were grown in Schneider medium (Sigma®) containing 20 μ g/L hemin (Sigma®), 10 μ g/mL folic acid (Sigma®) and 10% of fetal bovine serum (FBS) (Gibco-Thermo Fisher Scientific®). Passages were performed by addition of 5% volume inoculum in 25 cm² cultures flasks kept at 28 °C. Parasites were maintained through weekly passages up to a total of six passages, ensuring parasites virulence.

2.3.2. Cultivation of LLC-MK2 host cell line

The LLC-MK2 cell line (epithelial morphology) from the kidney of *Macaca mulatta* (ATCC® CCL-7 $^{\rm TM}$) was kept in 75cm² culture flasks, containing Dulbecco's Modified Eagle Medium (DMEM) (Sigma®) supplemented with 10% FBS, penicillin (100 U/mL) and streptomycin (130 U/mL). Cells were cultured at 37 °C in a 5% CO2 atmosphere. After the formation of confluent monolayers, cultures were treated with trypsin/EDTA solution to obtain subcultures of these cells. In the day before the experiments, 1×10^5 were plated in 96-well plates (Kasvi®) and cultured as above.

2.3.3. Anti-Leishmania activity

Complexes (1) and (2) were diluted in DMSO at a stock concentration of 50 mmol $\rm L^{-1}$ and stored at -22 °C. After 24 h of promastigote culture, complexes (1) and (2) were added directly to the culture medium containing the parasites, resulting in concentrations of 0.5, 1.0, 5.0, 10.0, 20.0, 25.0 and 50.0 μ mol $\rm L^{-1}$. The final concentration of DMSO (Dimethyl sulfoxide - Merck®) in the medium never exceeded 0.01% (ν / ν). Complexes were not added in the control group. The parasites were cultured in the presence of the complexes for up to 96 h. Aliquots were taken every 24 h for counting in a Neubauer chamber, after dilutions (1:10 and 1:100) in 4% of formaldehyde in PBS (phosphate buffered saline - 0.01 M / pH 7.2), using a phase-contrast optical microscope. IC₅₀ was calculated as previously described [22].

2.3.4. Host cell viability

LLC-MK2 cells cultured for 24 h on 96-well plates were treated for 48 h with different concentrations of each compound; compound (1): 100, 200, 300, 400, 500 $\mu mol~L^{-1}$; and compound (2): 1, 10, 20, 50, 200 $\mu mol~L^{-1}$. Each compound concentration was added to 3 wells containing cells. Negative and positive controls were performed by adding the same concentration of DMSO used in the highest compound concentration and 10% triton-x, respectively. After 48 h, MTT solution (5 mg/mL in PBS) was added to all the wells for 4 h at 37 °C. Subsequently, the solution was removed, MTT solvent (1:1 of DMSO in isopropanol) was added to the wells, the plate was covered with aluminum foil and shaked for 15 min. Reading was performed at an absorbance of 590 nm (plate reader spectrophotometer - Molecular Probes Versa Max).

2.3.5. Mitochondrial membrane potential of Leishmania amazonensis

Parasites were treated or not with complex (1) at 10 μ mol L⁻¹ for 96 h, and then washed with PBS and incubated for 20 min at 28 °C with JC-1 in Schneider medium (final concentration of 10 μ g/L). Labeled parasites were analyzed on a BD FACSCalibur. Parasite presented green and red fluorescence indicating low and elevated mitochondria membrane potential. Independent experiments were performed three times. Data are presented on dot plots of green and red fluorescence, percentage of events were generated by gates on intense red signal and were highlighted on size and granularity dot plots inferring size of these parasites.

2.3.6. Transmission electron microscopy

L. amazonensis promastigotes were treated or not with complex (1) (10 μ mol L⁻¹) for 72 h. Parasites were washed with serum-free medium and fixed with 2.5% glutaraldehyde and 4% recently prepared

formaldehyde in sodium cacodilate buffer (0.1 M, pH 7.2) for 2 h. Cells were washed with sodium cacodylate buffer and post-fixed with 1% osmium tetroxide, 1.6% potassium ferrocyanide and 5 mM calcium chloride in sodium cacodylate buffer for 1 h. Cells were dehydrated with acetone employing serial concentrations of 30%, 40%, 50%, 70% and 100%. Inclusion was performed with epoxy resin. Ultrafine sections were contrasted with uranyl acetate and lead citrate and observed in a Transmission Electron Microscope Jeol 1400 Plus, using voltage acceleration of 80 kV. [33]

2.3.7. Statistical analysis

The test data were expressed as mean \pm standard deviation. Experiments were repeated at least three times. The data were analyzed using the One-Way ANOVA test, followed by the Tukey test, using the Graphpad Prism 5 software. Statistical significance was considered when P < 0.05.

2.4. DFT calculations

The structure of complex (1) was built from the X-ray structure of complex (2) using the GaussView 6 program [34]. Both structures were optimized through Density functional theory (DFT) calculations using the Gaussian 16 program [35]. The unrestricted UB3LYP functional was utilized with a mixed basis set including LANL2TZ with pseudo potentials for Co and 6-311G(d,p) for all other atoms [36–44]. The dispersion effects were included using the Grimme's function with the Becke–Johnson damping effect (GD3BJ) [45]. The solvent effects of water were included using the polarizable continuum model (IEFPCM) [46,47]. Hessians were calculated at the same level of theory as the optimizations. Thermal, entropy and zero-point vibrational corrections were added to the final energies at 298 K and 1 atm used for the discussion.

2.5. In silico docking studies

To this date, structural data are not available for protein tyrosine phosphatase (PTP) from *Leishmania amazonensis*. In this sense, *in silico* analysis (binding mode) of complex (1) with PTP from L. *major* (LmPRL-1) [28] were carried out using the bioinformatic server Patchdock [48,49]. DFT optimized structural data of (1) was employed and the LmPRL-1 enzyme structural data was retrieved from the Protein Data Bank (PDB ID: 3S4O). All possible poses have been considered as starting points and the docking analysis were performed. The first 100 poses were refined through the FireDock algorithm [50,51] where the global minimum energy was found for the enzyme-complex adduct. The default parameters were used for the docking calculation. Visualization of the adducts were made, and further analyzed with ChimeraX v. 1.4 [52,53].

3. Results and discussion

3.1. Synthesis and structure of cobalt(II) coordination compounds

The new ligands HL1 and HL2 were designed to increase the biological activity of coordination compounds, by adding coumarin groups.

Coumarins belong to a family of large and extensively studied compounds containing 2H-1- benzopyran-2-one core structure, which consists of fused benzene and α -pyrone rings. As this heterocyclic system exhibit physicochemical properties and interesting biological activities reported in the literature [54,55], we decided to attach this group to the structure of the ligands. Furthermore, Leishmaniasis is the third most important vector-borne disease. Thus, there is an urgent need to develop new treatments for this disease [56,57].

The Co(II) complexes were obtained with the isomeric ligands HL1 and HL2; HL1 presents the group 4-hydroxycoumarin and the ligand HL2 presents the group 7-hydroxycoumarin. These ligands can be obtained by the reaction between their respective epoxides and the

secondary amine BMPA, at room temperature, with high yields (\approx 80%). RMN data confirm the synthesis of the ligands shown in Fig. 1S-6S, which was also confirmed for HL2 by the X-ray molecular structure solved to complex (2). The reactions between cobalt(II) chloride and HL1 and HL2, in methanol, resulted in green and light purple complexes, respectively, with very good yields. Complex (1) was obtained as a green solid. Complex (2) was obtained as crystalline material after the addition of LiClO₄ to the mother solution, resulting in monocrystals that allowed the molecular structure resolution by x-ray diffraction. The structure for complex (1) was proposed by elemental analysis (CHN), ESI-(+)-MS, electronic and infrared spectroscopies data, as well as based on that results obtained for complex (2). Furthermore, conductivity studies in solution suggested that complex (1) is a neutral species and complex (2) is cationic (1:1 electrolyte type), in CH₃CN. Both complexes are stable in air and soluble in polar solvents such as DMF, DMSO, CH₃CN, ethanol and methanol. They are insoluble in water. Data of ESI-(+)-MS suggest that both complexes form the same cationic mononuclear species in solution: $[M]^+ = 511$: $[Co(HL1)Cl]^+$ or $[Co(HL2)Cl]^+$. The chemical analysis indicate that complexes (1) and (2) are very distinct in solid state; complex (1) is neutral and presents two chloro ligands coordinated to the Co(II) centre. Complex (2), obtained as a cationic species, presents, further the ligand HL2, one chloro ligand and one methanol molecule coordinated to the Co(II) center, and a ClO₄ anion as counter-ion. Thus, infrared and electronic spectra for both are very different (Fig. 2S, 7S, 8S, and 17S). As a result of the isomerism of the ligand HL1 and HL2, differences in the biological activity of these complexes can be observed, as this is the first study employing these isomeric Co(II) complexes containing the groups 4 and 7-hydroxycoumarin. Thus, one aim of this work is to investigate the effect of isomerism on leishmanicidal activity.

3.1. Description of the crystal structure of the complex (2)

The single crystal X-ray diffraction analysis of complex (2) shows that the asymmetric unit consists of a mononuclear cobalt(II) complex and one perchlorate anion. A perspective view of the cation is displayed in Fig. 1. The bond lengths and angles for complex (2) are listed in Table 1. In (2), the cobalt center is coordinated by a σ –N₃O donor set provided by the ligand HL2 through one nitrogen atom from the amine (N2), two nitrogen atoms from pyridine (N1 and N3), one oxygen atom from the alcohol group (O1), one chloro ligand (Cl1) and a protonated O from the methanol molecule (O5), resulting in a hexacoordinated cobalt (II) complex. The geometry for Co(II) in complex (2) is described as distorted octahedral geometry. The axial positions are occupied by the nitrogen from the amine (N2) atom and by the chloro ligand (Cl1).

3.2. DFT calculations

Both complexes (1) and (2) were optimized using DFT calculations. They can exist in the doublet and quartet spin states. In the optimized structures for both states, electron spins were localized on the Co atom i. e. 0. 98e and 2.7e for the doublet and quartet states. The high spin quartet state was found to be the ground state for both complexes i.e. 10.7 and 12.9 kcal/mol lower in energy than the doublet state for complex 1 and 2, respectively. There are substantial differences in the metal-ligand bonds in these spin states (Fig. 2). The existence of the quartet state as a ground state of these complexes is also supported by the experimental data. Additionally, the geometrical parameters such as metal-ligand distances and bond angles of the optimized structure of complex (2) were in good agreement with the corresponding crystal structure (Table 4S). It validated the choice of DFT functional and basis set used in these calculations. The planer Co-N distances in both complexes were comparable. However, the axial Co-N3 bond in complex (1) is 0.05 Å longer than the corresponding distance in complex (2) (Table 5S).

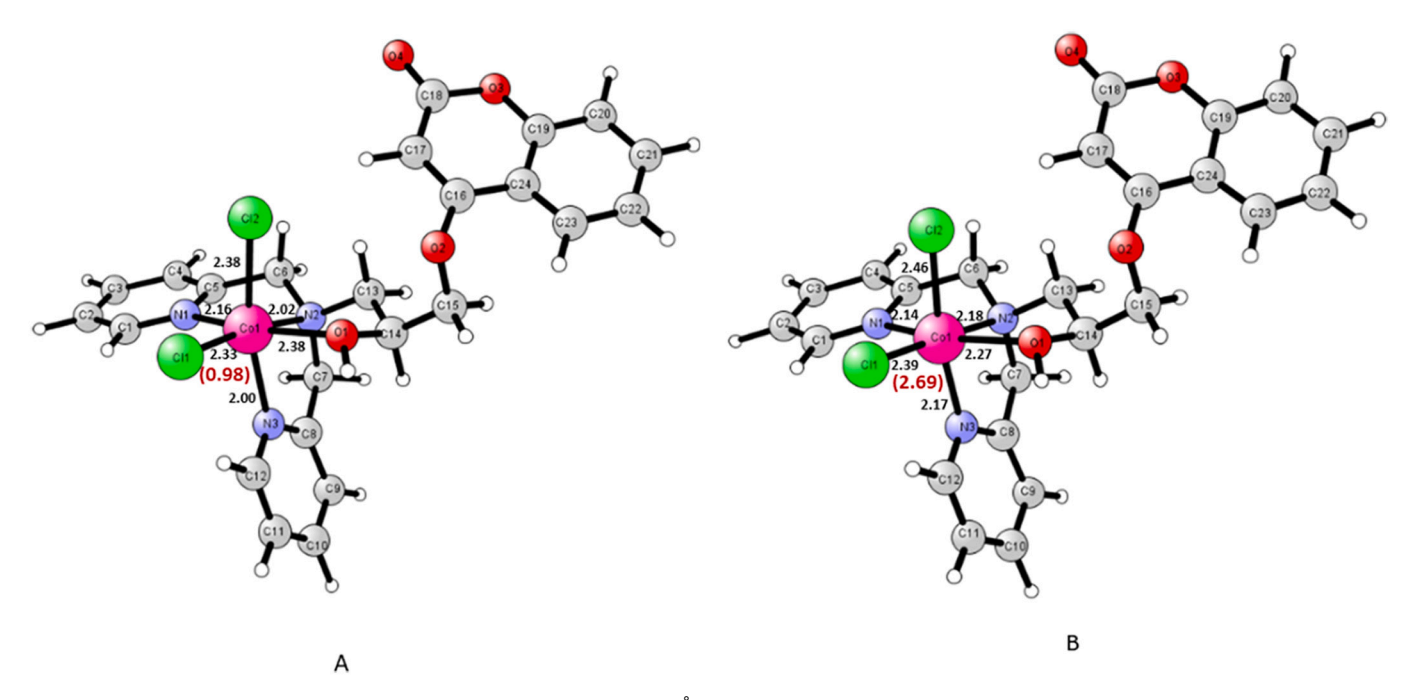


Fig. 2. DFT optimized structure of complex (1) with key distances (in Å) and electronic spin (in parenthesis): (A) doublet and (B) quartet spin state.

3.3. Infrared and electronic spectroscopies

The IR spectra of complexes (1) and (2) were analyzed in comparison with those of their free ligands. For all the complexes, the main bands showed shifts when compared to the respective free ligands (Fig. 7 and 8S). The bands related to ν C=O where shifted to lower energy (1731 to 1704 cm⁻¹) after coordination to cobalt(II) salt. The infrared spectrum of complex (1) displays typical bands of the ligand HL1, and complex (2) displays bands assignable to the ligand HL2 and the counter-ion ClO_4^- at 1132 cm⁻¹, which is absent in complex (1).

Fig. 3 shows the electronic spectrum of complex (2), in CH₃CN. The spectrum of complex (1) is presented in the supplementary material (Fig. 17S). The absorptions observed in the electronic spectra of the complexes are typical of d-d transition, as indicated by the low coefficient of molar extinction. This study suggests also that the electronic features of the complex (1) are significantly different from the complexes (2) which may indicate a different geometry for both complexes,

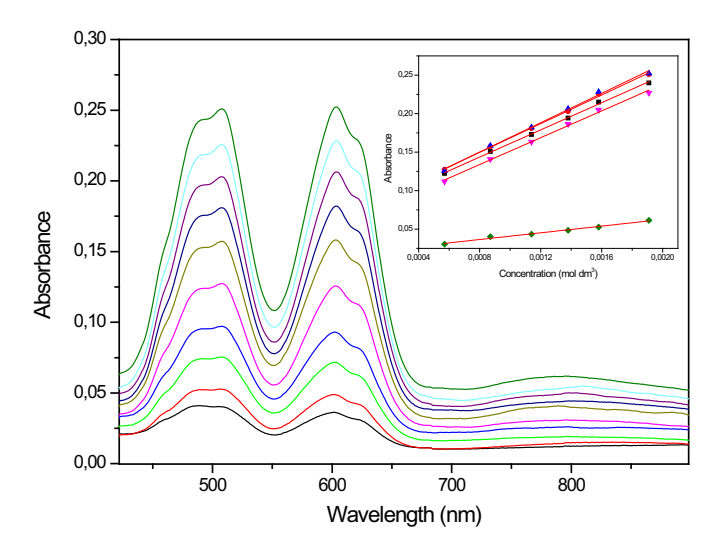


Fig. 3. Electronic spectrum of complex (2), obtained in CH_3CN , at the concentration range of 5.7 10^{-4} to 2.0 10^{-3} mol L^{-1} .

in solution.

3.4. ESI-(+)-MS and ESI-(+)-MS/MS

ESI-(+)-MS and ESI-(+)-MS/MS for the isomeric complexes (1) and (2) present a characteristic set of isotopologue ions due mainly to the presence of metal and Cl atoms. For complex (1) the ESI-(+)-MS data indicate the presence of one main peak with m/z 511, revealing the presence of a mononuclear complex in solution: $[Co(HL1)Cl]^+$ (Fig. 4). Fig. 10S presents the isotopic profile assignments for the peak observed in the ESI(+)-MS of complex (1) (Fig. 9S).

Fig. 11S presents the ESI(+)-MS spectrum of complex (2), in CH₃CN. For complex (2), ESI-(+)-MS data indicate the presence of identical peak with m/z 511, with additional peaks at m/z 475 and m/z 528. So, ESI-(+)-MS data suggest that complexes (1) and (2) should have the same main structure in solution: $[Co(HL1)Cl]^+$ and $[Co(HL2)Cl]^+$, respectively, both with m/z 511, since HL1 and HL2 are isomeric ligands. Fig. 12S presents the isotopic profile assignments for the peak at m/z 511 observed in the ESI(+)-MS of complex (2). The additional peaks at m/z 475 and 528, observed in the spectrum of complex (2), are ascribed to

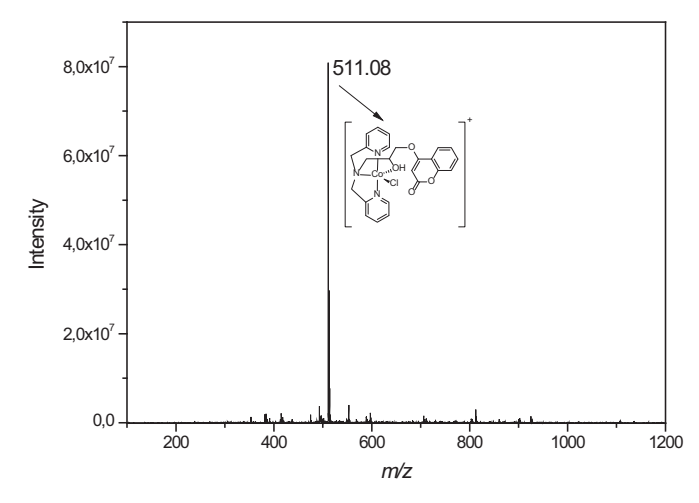


Fig. 4. ESI-(+)-MS spectrum of complex (1), in CH₃CN.

mononuclear complexes: $[Co(L2)]^+$ and $[Co(HL2)(OH)Cl]^+$ (with oxidation to Co(III)), respectively. Fig. 13 and 14S present the isotopic profile assignments for the peak at m/z 528 and 475, respectively, observed in the ESI-(+)-MS of complex **(2)**. ESI(+)-MS/MS data for complex **(2)** indicates that the species with m/z 511 yields the cation with m/z 475, attributed to $[Co(L1)]^+$. Fig. 15S shows the ESI(+)-MS/MS for the peak with m/z 511 and Fig. 16S presents the isotopic profile assignments for the peak at m/z 475 obtained by MS/MS of the signal of m/z 511, for complex **(2)**.

3.5. Anti-Leishmania activity and host cell viability

Complexes (1) and (2) were analyzed for their antiproliferative activity against promastigotes of L. *amazonensis*. Fig. 5A and B presents the cytotoxic effects of complex (1) and (2), respectively. The antiproliferative effect was higher as the concentration of both complexes and the time of treatment of both complexes increased. IC₅₀ for complex (1) were 4.90 (24 h), 2.50 (48 h), 3.80 (72 h) and 3.40 μ mol L⁻¹ (96 h), and for complex (2) were 2.90 (24 h), 4.20 (48 h), and 2.80 μ mol L⁻¹ (72 h).

The effect of complexes (1) and (2) on the viability of LLC-MK2 was investigated. Fig. 6A and B presents the effects of complex (1) and (2), respectively, on the viability activity of the host cell. Complex (1) was less toxic with reasonable viability at the concentrations of 500 μ mol L^{-1} . On the other hand, complex (2) exhibited very high cytotoxic effect, with a 65% reduction of the host cell viability with the concentrations of 10 μ mol L^{-1} . It is intriguing that these two compounds show so different citotoxicity on the host cell. This is an effect that have to be better studied in the future with other compounds to evaluate if it is dependent on the type of isomer (7-hydroxy-coumarin in (2) and 4-hydroxy-coumarin in (1)) or due to the presence of methanol in the

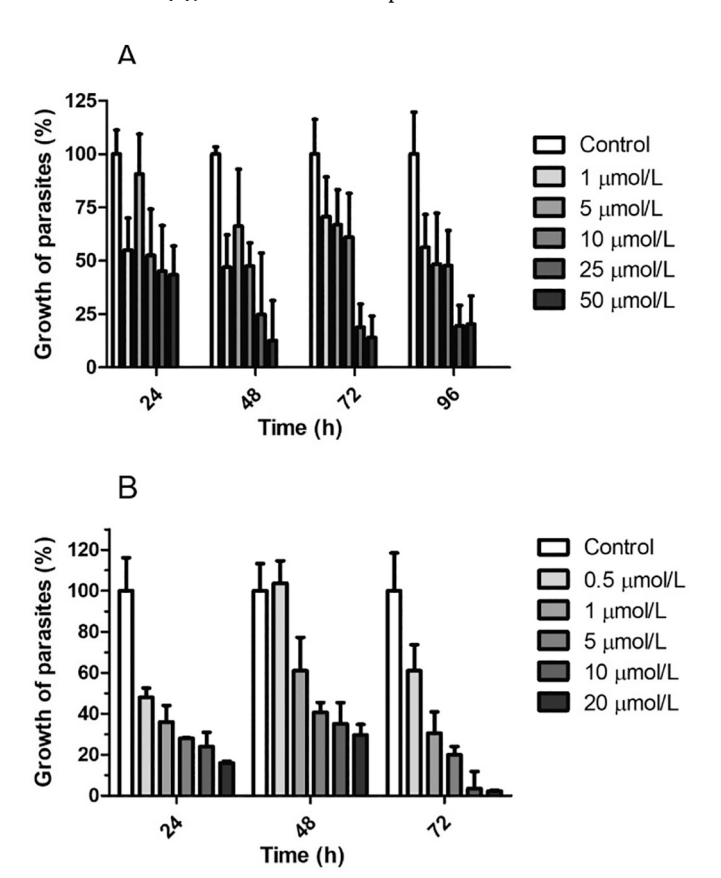


Fig. 5. Antiproliferative effects of complex **(1)** (A) and complex **(2)** (B) on promastigotes of *Leishmania amazonensis* with treatment times of 24 h, 48 h, 72 h and 96 h (only for complex **(1)**).

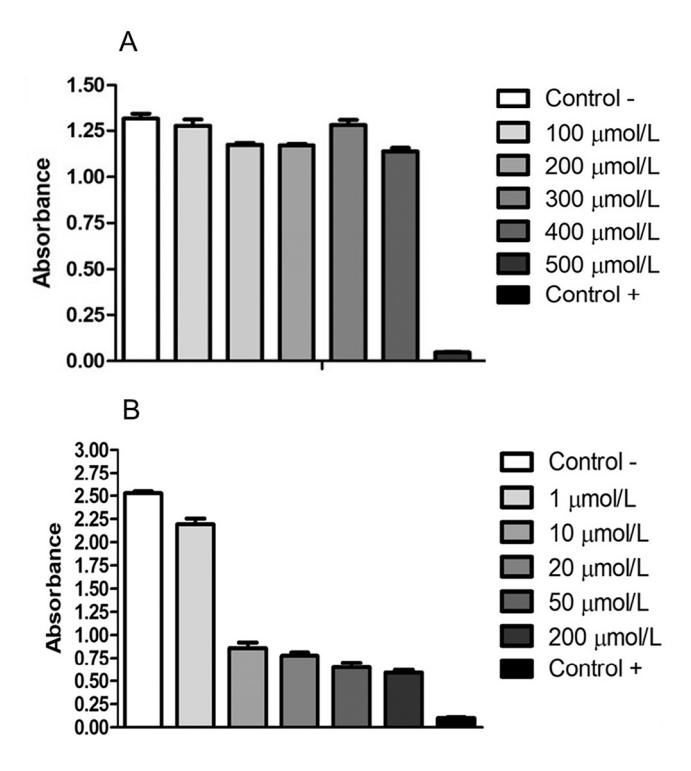


Fig. 6. Cytotoxic effects of complex **(1)** and **(2)** on LLC-MK2 by the MTT method. Absorbance of MTT crystals of viable LLC-MK2 treated with different concentrations of complex **(1)** (A) and **(2)** (B). Negative control: cells were cultured in DMEM with FBS without complexes; positive control: cells were cultured in DMEM with FBS without complexes containing 10% triton-x.

composition of complex (2).

Due to the higher toxicity to host cells of complex (2), further biological characterization was only performed with complex (1).

3.6. Mitochondrial activity

The effect of complex (1) on mitochondrial activity of the parasite was evaluated by visualizing the membrane potential of this organelle with the membrane-permeant JC-1 (5,5',6,6'-tetrachloro1,1',3,3'-tetramethylbenzimidazolylcarbocyanine iodide), a cationic dye, which has been used to monitor mitochondrial potential [58]. Leishmania presents a single mitochondria, an organelle that plays an important role in energy metabolism, and the dysfunction of this organelle can lead the parasite death. Fig. 7 shows that control parasites presents a low percentage of events on the dot plot gate drawn on the higher red fluorescence signal (FL2) and lower green fluorescence signal region (FL1) and parasites treated with complex (1) presented a seven fold increase on this gate. Events in these gates were highlighted in red color on SSC FSC dot pots showing their small size (Fig. 7, lower dot plots). Thus, the treatment with complex (1) induced mitochondria hyperpolarization and reduced the size of these parasites, which is associated with apoptosis, in accordance with previous results reported in the literature [59].

3.7. Analysis of cell morphology by transmission electron microscopy

To further understand how complex (1) was acting on the parasite, we analyzed the ultrastructure of the cells after treatment. Nontreated parasites presented normal ultrastructure with typical kinetoplast and nuclear aspects (Fig. 8A, B). After treatment, parasites presented altered kinetoplast with swelling of the mitochondria (Fig. 8C and D). This corroborates the higher mitochondria membrane potential observed after treatment with this complex and smaller size of the parasites. Thus,

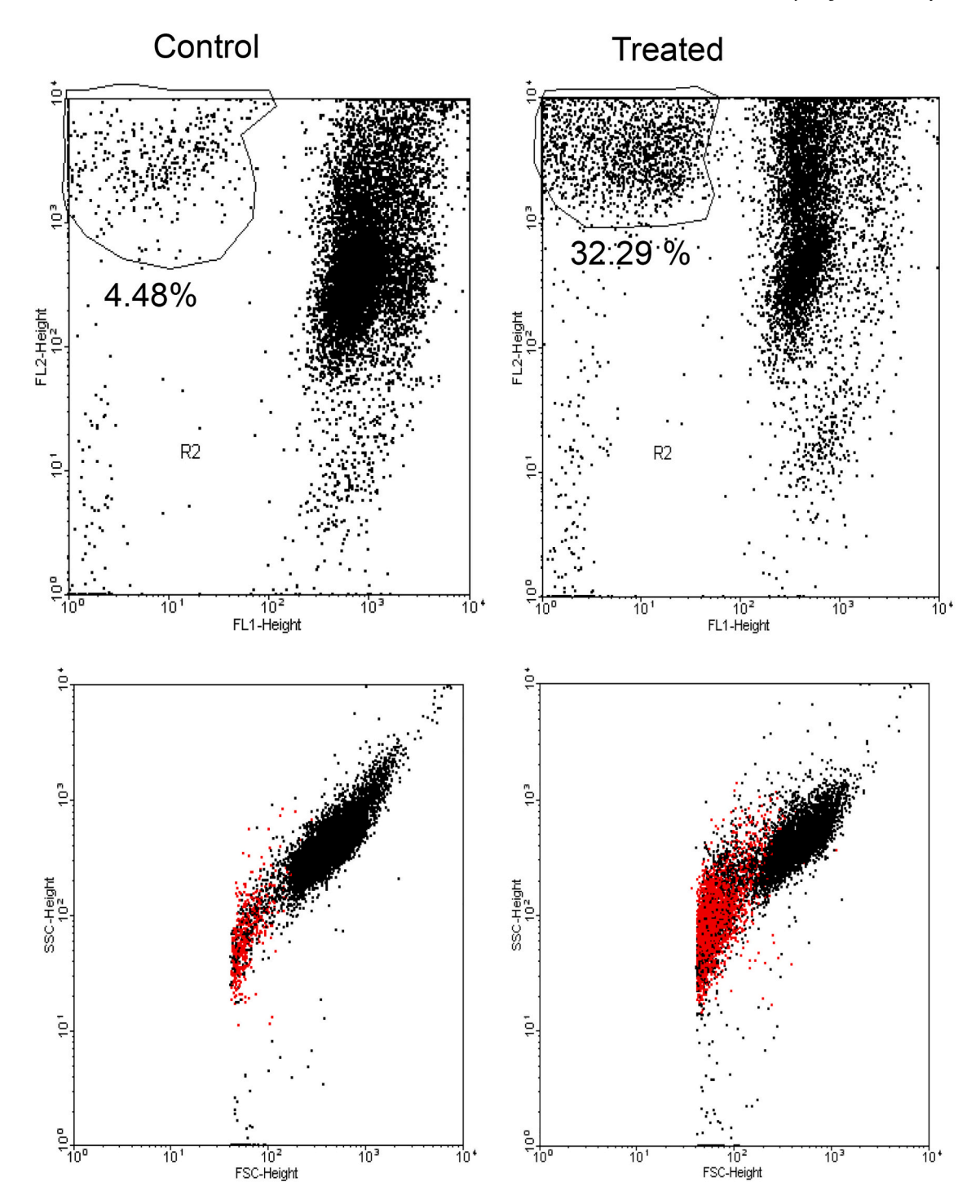


Fig. 7. Effect of complex (1) on mitochondrial membrane potential of promastigotes of *Leishmania amazonensis*. Parasites were not treated (control) or treated with complex (1) for 96 h. Control parasites show low percentage of events on higher red fluorescence signal (FL2)/lower green fluorescence signal and treated parasites presented more events in this gate. Percentage of events were calculated in gates and highlighted in red color on SSC FSC dot pots. (For interpretation of the references to color in this figure legend, the reader is referred to the web version of this article.)

complex (1) was able to alter the structure and function of this important organelle. We also observed degraded bodies of the parasite (Fig. 8E), indicating death by necrosis. In addition, parasites presented plasma membrane bleb (Fig. 8F), chromatin concentrated in patches at the nuclear envelop (Fig. 8G and H) and degenerated chromatin (Fig. 8I). These are typical morphological characteristics of cell death promoted by apoptosis-like in trypanosomes [60,61]. Therefore, complex (1) may be acting on the mitochondria and inducing an apoptotic-like cell death process on the parasite. The effect of complex (1) on

mitochondria adds to similar outcomes described by different metallic complexes [18,22,23]. Therefore, these complexes may be causing cell stress resulting in mitochondrial changes, which may induce, by the intrinsic pathway, apoptosis-like cell death.

3.8. In silico docking studies of complex (1) upon the LmPRL-1

Protein tyrosine phosphatase secreted by L. *major* (LmPRL-1) consist in a hydrolase which has crucial role in regulating the proliferation,

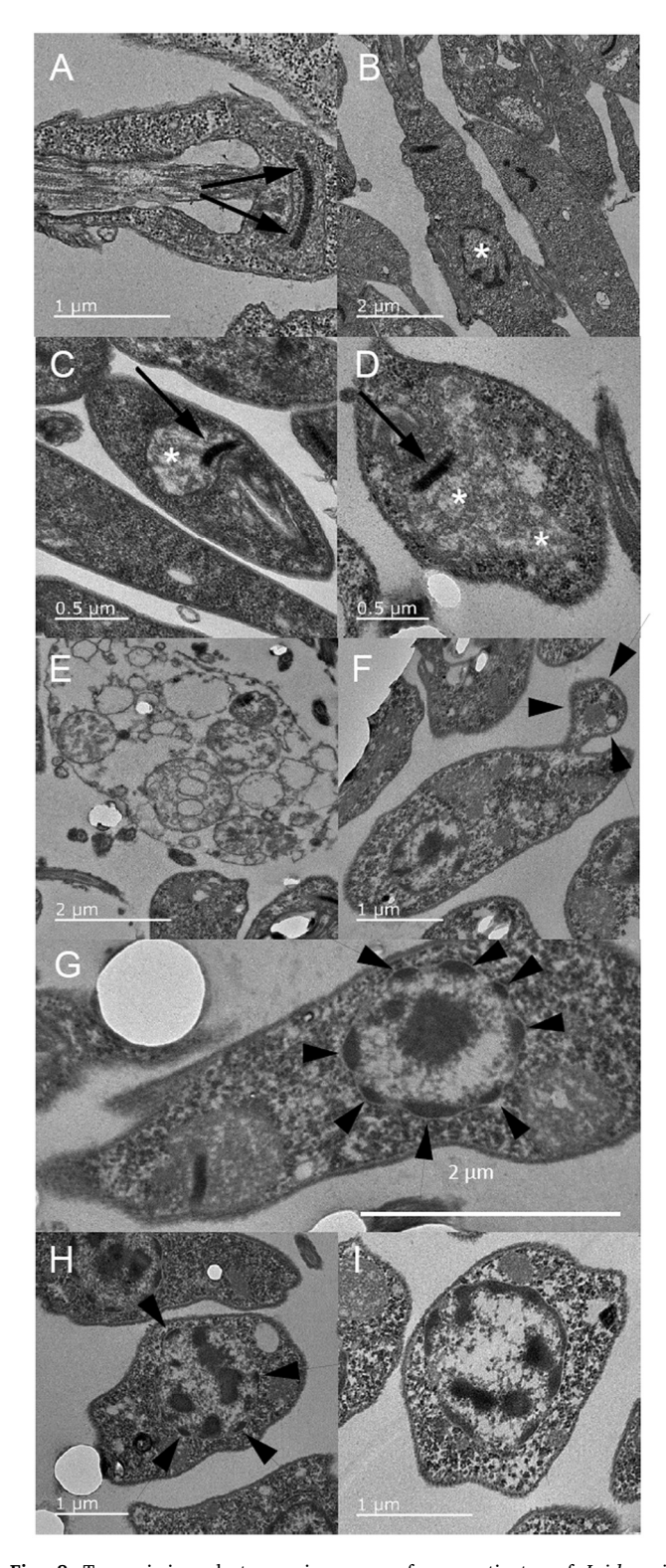


Fig. 8. Transmission electron microscopy of promastigotes of *Leishmania amazonensis* treated or not with complex **(1)**. (A, B) Control parasites without complex treatment. Normal appearance of the parasite kinetoplast (arrows) and nucleus (*). (C to I) Complex **(1)** treated parasites for 72 h presented altered kinetoplast structure (C, D - arrow), with clear swelling of the mitochondria (*), degeneration of the cell body (E), plasma membrane bleb at the parasite surface (F - arrowheads), and altered nucleus structure, with chromatin concentrated in patches at the nuclear envelop (G, H - arrowheads) and degenerated chromatin (I).

differentiation, and motility of cells. This enzyme is predominantly expressed and secreted by promastigotes *via* the exosome route then, its inhibition constitutes a strategical target to fight against the parasite [28]. In order to visualize the plausible interaction between the complex (1) herein studied and LmPRL-1 (PDB code: 3S4O), molecular docking simulations were performed. The most favorable docked pose is illustrated in Fig. 9.

As depicted in Fig. 9 (top, left), complex (1) could dock into the enzyme surface through a hydrophobic pocket, close to the catalytic active site. One of the pyridine rings of complex (1) is approx. 10 Å to the catalytic (CYS116) and the regulatory (CYS55) cysteines located into the Loop-2 and P-Loop, respectively (top, right and bottom). Pyridine and the coumarin rings from complex (1) can interact with LmPRL-1 with THR58, MSE5 and ASN6 residues, respectively. The nature of these interactions is hydrophobic (Van der Waals forces) with the distance between 2.9 and 3.4 Å. A plausible hydrogen bond (3.164 Å) can be observed between the coumarin out-of-ring oxygen and the NH group of SER32 (peptide bond). The interaction distances are depicted in Fig. 9 (bottom, yellow dashed lines).

The structure of complex (1), selected for *in silico* docking studies, upon the LmPRL-1 (Fig. 9) presents two chloro ligands coordinated to the Co(II) center, according to DFT data. These labile ligands are changed by DMSO or phosphate groups, in agreement with electrical conductivity and stability studies, performed in CH_3CN , DMSO or 0.1% DMSO, in PBS buffer or by components of the Schneider medium (Fig. 17, 18 and 19S). The interactions with LmPRL-1 will be very

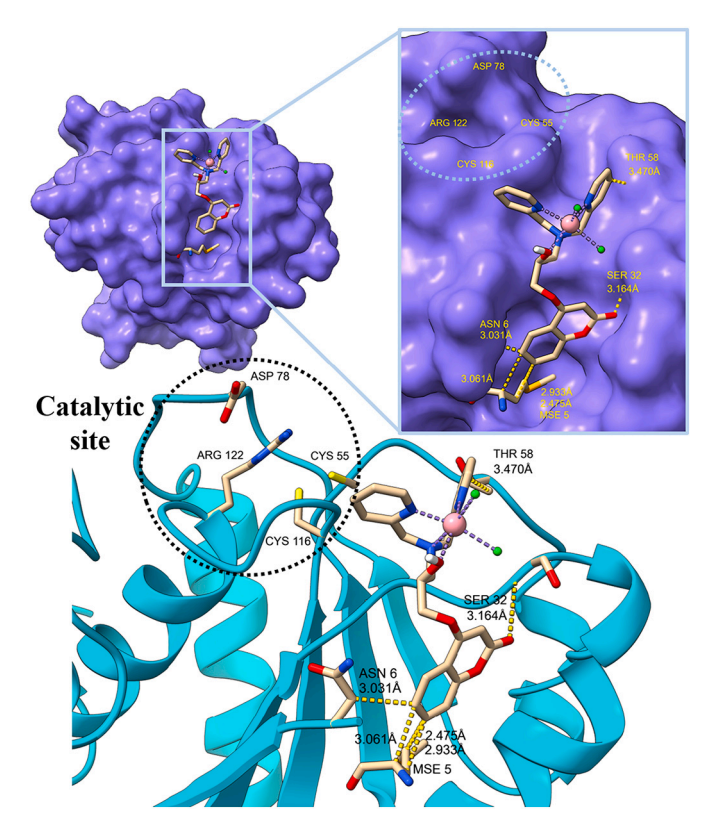


Fig. 9. Best refined docking pose of complex (1) and LmPRL-1 (PDB: 3S4O), considering the surface representation of the enzyme (top, left). Zoomed region presenting the proximity of the active site (dashed circle) and the docking region where (1) is lodged (top right). Cartoon representation of the enzyme (cyan) where active site and the interactions between (1) and the LmPRL-1 are shown (bottom). Atom colors: Carbon, grey; oxygen, red; nitrogen, blue; green, chlorine; yellow, sulfur and pink, cobalt). Wan der Waals and hydrogen bonds are represented by dashed yellow lines. (For interpretation of the references to color in this figure legend, the reader is referred to the web version of this article.)

similar, considering chloro ligands or DMSO coordinated to the Co(II) center, since these groups are out of the enzyme pocket.

Inhibition of protein tyrosine phosphatases (PTPs) are subject of intense *in vitro* studies once it is related to a series of metabolic disfunctions and diseases [62]. Specifically, docking studies of oxo-vanadium [63,64], copper [65], zinc and iron complexes [66] have been performed and strong activity inhibition was observed. In these cases, metal complexes could inhibit the enzyme activity by blocking their catalytic site or by docking into different allosteric spots all over the protein surface.

4. Conclusions

In this report we have introduced two new mononuclear Co(II) complexes. The coumarin group is presented in the structures of both complexes, confirmed by X-ray diffraction studies for complex (2), which presents the group 7-hydroxy-coumarin while complex (1) presents the group 4-hydroxy-coumarin. Both ligands and complexes were completely characterized and this work presents, for the first time, the leishmanicidal activity of these Co(II) complexes obtained with these isomeric ligands HL1 and HL2.

Complex **(1)** presented no cytotoxicity to the LLC-MK2 host cells, but complex **(2)** was toxic. IC₅₀ for complex **(1)** were 4.90 μ mol L⁻¹ (24 h), 3.50 μ mol L⁻¹ (48 h) and 3.80 μ mol L⁻¹ (72 h), 3.40 (96 h) and for complex **(2)** were 2.09 μ mol L⁻¹ (24 h), 4.20 μ mol L⁻¹ (48 h), and 2.80 μ mol L⁻¹ (72 h) against the promastigote form of L. *amazonensis*. The high cytotoxicity of complex **(2)** toward host cells demonstrates the effect of the isomerism of the ligand, which modulates the biological activity.

The mechanism of cell death promoted by complex (1) was investigated by analysis of mitochondrial membrane potential and transmission electron microscopy, which suggests that the apoptosis-like cell death is directly related to mitochondrial dysfunction.

Our work established that the structure of the ligand shows a crucial effect on the cytotoxicity and reveals the importance of studies containing different isomers.

To the best of our knowledge, this is the first example of metal complex that had its *in silico* docking properties tested upon PTP from L. *major*. Despite complex (1) did not dock into the active site pocket, its presence near to it could trigger a non-competitive enzyme inhibition process for example.

CRediT authorship contribution statement

Samuel M. Rocha: synthesis and characterization of ligands and coordination compounds (spectroscopic, structural and electrochemical characterization), writing, preparation of tables, figures and the supplementary material, obtaining compound (2) in crystalline form. Adolfo Horn Jr.: work design, manuscript writing, review and editing, funding acquisition. Aline R. de M. L. Terra, Lara M. Rezende, Felipe F. Moreira, Renato A. DaMatta and Sérgio H. Seabra: in vitro antitoxoplasma activity and light microscopy images, writing and review. Fernando R. Xavier: docking molecular studies, writing and review. Roberta Cargnelutti and Rodrigo Cervo: X-ray diffraction studies for complex (2), writing and review. Sreerag N. Moorkkannur, Graysen Owenby and Rajeev Prabhakar: DFT studies, manuscript writing and review. Christiane Fernandes: conception of the work, funding acquisition, writing of the manuscript, supervision of Samuel M. Rocha, contact with collaborators, organization of the manuscript and coordination of the review stage and submission.

Declaration of Competing Interest

The authors declare that they have no known competing financial interests or personal relationships that could have appeared to influence the work reported in this paper.

Data availability

Data will be made available on request.

Acknowledgements

This work was also financed in part by the Coordenação de Aperfeiçoamento de Pessoal de Nível Superior - Brasil (CAPES) - Finance Code 001.We thank LABIME (Laboratório de Biologia Molecular e Estrutural- UFSC) by the ESI-(+)-MS and ESI-(+)-MS/MS analysis, and Central de Análises- UFSC. SHS was financed by Fundação Carlos Chagas Filho de Amparo à Pesquisa do Estado do Rio de Janeiro -FAPERJ- (E-26/211.850/2021) and RAD by Conselho Nacional de Desenvolvimento Científico e Tecnológico -CNPq- (317528/2021-1) and FAPERJ (E-26/200.980/2021). FRX was financed by the Fundação de Amparo à Pesquisa e Inovação do Estado de Santa Catarina -FAPESC- 2021TR964. This material is based upon work supported by a grant from the National Science Foundation (Grant Number CHE- 2102563) to R.P.

Appendix A. Supplementary data

Supplementary data to this article can be found online at $\frac{\text{https:}}{\text{doi.}}$ org/10.1016/j.jinorgbio.2022.112088.

References

- P.D. Marsden, Mucosal leishmaniasis ("espundia" Escomel, 1911), R. Soc. Trop. Mucosal Leishmaniasis 80 (1986) 859–876, https://doi.org/10.1016/0035-9203 (86)90243-9
- [2] R.W. Ashford, The leishmaniases as emerging and reemerging zoonoses, Int. J. Parasitol. 30 (2000) 1269–1281, https://doi.org/10.1016/S0020-7519(00)00136-3.
- [3] World Health Organization-WHO, Leishmaniasis. www.who.int/leishmaniasis/disease/en/, 2020 (Accessed 13 june 2022).
- [4] D.E. Teixeira, M. Benchimol, J.C.F. Rodrigues, P.H. Crepaldi, The cell biology of Leishmania: how to teach using animations, Pathogens 9 (2013) 7–11, https://doi. org/10.1371/journal.ppat.1003594.
- [5] E. Mougneau, F. Bihl, N. Glaichenhaus, Cell biology and immunology of Leishmania, Immunol. Rev. 240 (2011) 286–296, https://doi.org/10.1111/j.1600-065X 2010 00983 x
- [6] P. Kaye, P. Scott, Leishmaniasis: complexity at the host pathogen interface, Nat. Rev. Microbiol. 9 (2011) 604–615, https://doi.org/10.1038/nrmicro2608.
- [7] D. Ashok, H. Acha-Orbea, Timing is everything: dendritic cell subsets in murine Leishmania infection, Trends Parasitol. 10 (2014) 499–507, https://doi.org/ 10.1016/j.pt.2014.08.001.
- [8] T.D. Souza, A.P. Turchetti, R.T. Fujiwara, et al., Visceral leishmaniasis in zoo and wildlife, Vet. Parasitol. 200 (2014) 233–241, https://doi.org/10.1016/j. vetpar.2013.12.025.
- [9] K. Bi, Y. Chen, S. Zhao, Y. Kuang, C.-H.J. Wu, Current visceral Leishmaniasis research: a research review to inspire future study, Biomed. Res. Int. ID (2018) 9872095, https://doi.org/10.1155/2018/9872095.
- [10] D. Savoia, Recents updates and perspectives on leishmaniases, J. Infect. Dev. Count. 9 (2015) 588–596, https://doi.org/10.3855/jidc.6833.
- [11] F.T. Silveira, R. Lainson, C.M.D.E.C. Gomes, M.D. Laurenti, C.E.P. Corbett, Immunopathogenic competences of *Leishmania* (V.) *braziliensis* and *L. (L.) amazonensis* in American cutaneous leishmaniasis, Parasite Immunol. 31 (2009) 423–431, https://doi.org/10.1111/j.1365-3024.2009.01116.x.
- [12] M. Rossi, N. Fasel, How to master the host immune system? Leishmania parasites have the solutions!, Int. Immunol. 30 (2017) 103–111, https://doi.org/10.1093/ intimm/dxx075.
- [13] A.C. Costa-da-Silva, D. Nascimento, J.R.M. Ferreira, K. Guimarães-Pinto, L. Freire-de-Lima, A. Morrot, D. Decote-Ricardo, A.A. Filardy, C.G. Freire-de-Lima, Immune responses in Leishmaniasis: an overview, Trop. Med. Infect. Dis. 7 (2022) 2–16, https://doi.org/10.3390/tropicalmed7040054.
- [14] J.T. Mesquita, A.G. Tempone, J.Q. Reimão, Combination therapy with nitazoxanide and amphotericin B, Glucantime®, miltefosine and sitamaquine against *Leishmania* (*Leishmania*) infantum intracellular amastigotes, Acta Trop. 130 (2014) 112–116, https://doi.org/10.1016/j.actatropica.2013.11.003.
- [15] W. de Souza, Protozoologia Médica, Rubio, Rio de Janeiro, 2013.
- [16] P. Layegh, O. Rajabi, M.R. Jafari, P.E.T. Malekshah, T. Moghiman, H. Ashraf, R. Salari, Efficacy of topical liposomal amphotericin B versus Intralesional Meglumine Antimoniate (Glucantime) in the treatment of cutaneous Leishmaniasis, J. Parasitol. Res. 2011 (2011), https://doi.org/10.1155/2011/ 656523
- [17] M. Vieites, P. Smircich, L. Guggeri, E. Marchán, A. Gómez-barrio, M. Navarro, B. Garat, D. Gambino, Synthesis and characterization of a pyridine-2-thiol N-oxide gold(I) complex with potent antiproliferative effect against *Trypanosoma cruzi* and

- Leishmania sp. insight into its mechanism of action, J. Inorg. Biochem. 103 (2009) 1300–1306, https://doi.org/10.1016/j.jinorgbio.2009.02.011.
- [18] M. Soares, Y. Garcia, S. Cota, D. Cristina, D.O. Nunes, D. Silva, C. Vieira, M. Santos, B. Cristina, M. José, B. Silva, R. Santos, V. De Melo, G. Von Poelhsitz, K. Aparecida, G. Yoneyama, Increased ROS generation causes apoptosis-like death: mechanistic insights into the anti- Leishmania activity of a potent ruthenium(II) complex, J. Inorg. Biochem. 195 (2019) 1–12, https://doi.org/10.1016/j.jinorgbio.2019.03.005.
- [19] J.A. Portes, T.G. Souza, T.A.T. Dos Santos, L.L.R. Da Silva, T.P. Ribeiro, M. D. Pereira, A. Horn Jr., C. Fernandes, R.A. Da Matta, W. de Souza, S.H. Seabra, Reduction of toxoplasma gondii development due to inhibition of parasite antioxidant enzymes by a dinuclear iron(III) compound, Antimicrob. Agents Chemother. 59 (2015) 7374–7386, https://doi.org/10.1128/AAC.00057-15.
- [20] V.M. de Assis, L.C. Visentin, F.S. de Souza, A.R. DaMatta, A. Horn Jr., A. C. Fernandes, Synthesis, crystal structure and relevant antiproliferative activity against toxoplasma gondii of a new binuclear co(II) complex, Inorg. Chem. Commun. 67 (2016) 47–50, https://doi.org/10.1016/j.inoche.2016.02.017.
- [21] J.A. Portes, C.S. Motta, N.F Azeredo, C. Fernandes, A. Horn Jr, W. Souza, R.A. DaMatta, S.H. Seabra, *In vitro* treatment of *toxoplasma gondii* with copper(II) complexes induces apoptosis-like and cellular division alterations, Vet. Parasitol., 245, 2017, 141–152. doi: https://doi.org/10.1016/j.vetpar.2017.04.002.
- [22] F.F. Moreira, J.A. Portes, N.F.B. Azeredo, C. Fernandes, A. Horn Jr., C.P. Santiago, B.B. Segat, G.F. Caramori, L.M.P. Madureira, D.R.S. Candela, M.M. Marques, J.A.L. C. Resende, W. de Souza, R.A. Da Matta, S.H. Seabra, Development of new dinuclear Fe(III) coordination compounds with in vitro nanomolar antitrypanosomal activity, Dalton Trans. (2021), https://doi.org/10.1039/d14001048d
- [23] A.P. Cardoso, L.M.P. Madureira, Bruna B. Segat, N.C. Jennifer, Roberta Cargnelutti, Dalber R.S. Candela, Davor L. Mariano, Renato L.T. Parreira, Adolfo Horn Jr., Sérgio H. Seabra, Renato A. DaMatta, Felipe F. Moreira, Renata V. Moreira, F. Giovanni, Caramori, Christiane Fernandes, Development, structural, spectroscopic and in silico investigation of new complexes relevant as antitoxoplasma metallopharmacs, J. Mol. Struct. 1265 (2022) 133380, https://doi. org/10.1016/j.molstruc.2022.133380.
- [24] G.A. Gonçalves, A.R. Spillere, G.M. das Neves, L.P. Kagami, G.L. von Poser, R.F. S. Canto, V. Eifler-Lima, Natural and synthetic coumarins as antileishmanial agents: a review, Eur. J. Med. Chem. 203 (2020), 112514, https://doi.org/10.1016/j.ejmech.2020.112514.
- [25] B. Rostom, R. Karaky, I. Kassab, M.S. Veitía, Coumarins derivatives and inflammation: review of their effects on the inflammatory signaling pathways, Eur. J. Pharmacol. 92 (2022), 174867, https://doi.org/10.1016/j.ejphar.2022.174867.
- [26] V. Mandlik, S. Patil, R. Bopanna, S. Basu, S. Singh, Biological activity of Coumarin derivatives as anti-leishmanial agents, PLoS One 11 (2016) 1–15, https://doi.org/ 10.1371/journal.pone.0164585.
- [27] S. Parveen, F. Arjmand, S. Tabassum, Development and future prospects of selective organometallic compounds as anticancer drug candidates exhibiting novel modes of action, Eur. J. Med. Chem. 175 (2019) 269–286, https://doi.org/ 10.1016/j.ejmech.2019.04.062
- [28] L. Balewski, S. Szulta, A. Jali, A. Kornicka, A mini-review: recent advances in coumarin-metal complexes with biological properties, Front. Chem. 9 (2021) 1–18, https://doi.org/10.3389/fchem.2021.781779.
- [29] S. Leitherer, J. Clos, E.M. Liebler-Tenorio, U. Schleicher, C. Bogdan, D. Soulat, Characterization of the protein tyrosine phosphatase LmPRL-1 secreted by Leishmania major via the exosome pathway, Infect. Immun. 85 (2017), https://doi. org/10.1128/2FIAI.00084-17 e00084-17.
- [30] G.M. Sheldrick, Crystal structure refinement with SHELXL, Acta Crystallographica section C, Struct. Chem. 71 (1) (2015) 3–8, https://doi.org/10.1107/ \$2053229614024218
- [31] G.M. Sheldrick, A short history of SHELXL, Acta Crystallogr. Sect. A. 64 (2008) 112–122, https://doi.org/10.1107/S0108767307043930.
- 112–122, https://doi.org/10.1107/S0108767307043930.
 [32] K. Brandenburg, H. Putz, Diamond Crystal and Molecular Structure Visualization (Version 4.6.0). Crystal Impact GbR- Bonn, Germany, 2019.
- [33] A. Neves, M.A. de Brito, I. Vencato, Synthesis, crystal structure and properties of a new binuclear Iron(III) complexes as a model for the purple acid phosphatase, Inorg. Chim. Acta 214 (1993) 5–8, https://doi.org/10.1016/S0020-1693(00)
- [34] M. Poot, Y.Z. Zhang, J.A. Kramer, K.S. Wells, L.J. Jones, D.K. Hanzel, A.G. Lugade, V.L. Singer, R.P. Haugland, Analysis of mitochondrial morphology and function with novel fixable fluorescent stains, J. Histochem. Cytochem. 44 (1996) 1363–1372, https://doi.org/10.1177/44.12.8985128.
- [35] R. Dennington, T.A. Keith, J.M. Millam, Semichem Inc., Shawnee Mission, KS, 2016.
- [36] M.J. Frisch, G.W. Trucks, H.B. Schlegel, G.E. Scuseria, M.A. Robb, J.R. Cheeseman, G. Scalmani, V. Barone, G.A. Petersson, H. Nakatsuji, X. Li, M. Caricato, A. V. Marenich, J. Bloino, B.G. Janesko, R. Gomperts, B. Mennucci, H.P. Hratchian, J. V. Ortiz, A.F. Izmaylov, J.L. Sonnenberg, F. Ding, F. Lipparini, F. Egidi, J. Goings, B. Peng, A. Petrone, T. Henderson, D. Ranasinghe, V.G. Zakrzewski, J. Gao, N. Rega, G. Zheng, W. Liang, M. Hada, M. Ehara, K. Toyota, R. Fukuda, J. Hasegawa, M. Ishida, T. Nakajima, Y. Honda, O. Kitao, H. Nakai, T. Vreven, K. Throssell, J.A. Montgomery Jr., J.E. Peralta, F. Ogliaro, M.J. Bearpark, J. J. Heyd, E.N. Brothers, K.N. Kudin, V.N. Staroverov, T.A. Keith, R. Kobayashi, J. Normand, K. Raghavachari, A.P. Rendell, J.C. Burant, S.S. Iyengar, J. Tomasi, M. Cossi, J.M. Millam, M. Klene, C. Adamo, R. Cammi, J.W. Ochterski, R.L. Martin, K. Morokuma, O. Farkas, J.B. Foresman, D.J. Fox, Gaussian 16 Rev. C.01, Wallingford, CT, 2016.

- [37] C. Lee, W. Yang, R.G. Parr, Development of the Colle-Salvetti correlation-energy formula into a functional of the electron density, Phys. Rev. B 37 (1988) 785–789, https://doi.org/10.1103/physrevb.37.785.
- [38] B.P. Pritchard, D. Altarawy, B. Didier, T.D. Gibson, T.L. Windus, New basis set exchange: an open, up-to-date resource for the molecular sciences community, J. Chem. Inf. Model. 59 (2019) 4814–4820, https://doi.org/10.1021/acs. icim.9b00725.
- [39] D. Feller, The role of databases in support of computational chemistry calculations, J. Comput. Chem. 17 (1996) 1571–1586, https://doi.org/10.1002/(SICI)1096-987X(199610)17:13<1571::AID-JCC9>3.0.CO;2-P.
- [40] K.L. Schuchardt, B.T. Didier, T. Elsethagen, L. Sun, V. Gurumoorthi, J. Chase, J. Li, T.L. Windus, Basis set exchange: a community database for computational sciences, J. Chem. Inf. Model. 47 (2007) 1045–1052, https://doi.org/10.1021/ci600510j.
- [41] P.J. Hay, W.R. Wadt, Ab initio effective core potentials for molecular calculations. Potentials for K to Au including the outermost core orbitals, J. Chem. Phys. 82 (1985) 299–310, https://doi.org/10.1063/1.448975.
- [42] L.E. Roy, P.J. Hay, R.L. Martin, Revised basis sets for the LANL effective core potentials, J. Chem. Theory Comput. 4 (2008) 1029–1031, https://doi.org/ 10.1021/ct8000409
- [43] M.M. Francl, W.J. Pietro, W.J. Hehre, J.S. Binkley, M.S. Gordon, D.J. DeFrees, J. A. Pople, Self-consistent molecular orbital methods. XXIII. A polarization-type basis set for second-row elements, J. Chem. Phys. 77 (1982) 3654–3665, https://doi.org/10.1063/1.444267.
- [44] R. Krishnan, J.S. Binkley, R. Seeger, J.A. Pople, Self-consistent molecular orbital methods. XX. A basis set for correlated wave functions, J. Chem. Phys. 72 (1980) 650–654, https://doi.org/10.1063/1.438955.
- [45] A.D. McLean, G.S. Chandler, Contracted Gaussian basis sets for molecular calculations. I. Second row atoms, Z=11-18, J. Chem. Phys. 72 (1980) 5639-5648, https://doi.org/10.1063/1.438980.
- [46] S. Grimme, S. Ehrlich, L. Goerigk, Effect of the damping function in dispersion corrected density functional theory, J. Comput. Chem. 32 (2011) 1456–1465, https://doi.org/10.1002/icc.21759.
- [47] S. Miertuš, E. Scrocco, J. Tomasi, Electrostatic interaction of a solute with a continuum. A direct utilizaion of AB initio molecular potentials for the prevision of solvent effects, Chem. Phys. 55 (1981) 117–129, https://doi.org/10.1016/0301-0104(81)85090-2.
- [48] R. Cammi, J. Tomasi, Remarks on the use of the apparent surface charges (ASC) methods in solvation problems: iterative versus matrix-inversion procedures and the renormalization of the apparent charges, J. Comput. Chem. 16 (1995) 1449-1458. https://doi.org/10.1102/jcc.540161202
- 1449–1458, https://doi.org/10.1002/jcc.540161202.
 [49] D. Duhovny, R. Nussinov, H.J. Wolfson, Efficient unbound docking of rigid molecules, Lect. Notes Comput. Sci 2452 (2002) 185–200, https://doi.org/10.1007/3-540-45784-4.14
- [50] D. Schneidman-Duhovny, Y. Inbar, R. Nussinov, H.J. Wolfson, PatchDock and SymmDock: servers for rigid and symmetric docking, Nucleic Acids Res. 33 (2005), https://doi.org/10.1093/NAR/GKI481.
- [51] N. Andrusier, R. Nussinov, H.J. Wolfson, FireDock: fast interaction refinement in molecular docking, Proteins 69 (2007) 139–159, https://doi.org/10.1002/ prot. 21495
- [52] E. Mashiach, D. Schneidman-Duhovny, N. Andrusier, R. Nussinov, H. J. Wolfson, FireDock: a web server for fast interaction refinement in molecular docking, Nucleic Acids Res., 36, W229–32. doi: https://doi.org/10.1093/2Fnar/2Fgkn186.
- [53] E.F. Pettersen, T.D. Goddard, C.C. Huang, E.C. Meng, G.S. Couch, T.I. Croll, J. H. Morris, T.E. Ferrin, U.C.S.F. ChimeraX, Structure visualization for researchers, educators, and developers, Protein Sci. 30 (2021) 70–82, https://doi.org/10.1002/ pro.3943.
- [54] C.C. Huang, E.C. Meng, E.F. Pettersen, G.S. Couch, J.H. Morris, T.E. Ferrin, U.C.S. F. ChimeraX, Meeting modern challenges in visualization and analysis, Protein Sci. 27 (2018) 14–25, https://doi.org/10.1002/pro.3235.
- [55] T. Sarkar, A. Kumar, S. Sahoo, A. Hussain, Mixed-ligand cobalt(III) complexes of a naturally occurring Coumarin and Phenanthroline bases as mitochondria-targeted dual-purpose Photochemotherapeutics, Inorg. Chem. 60 (2021) 6649–6662, https://doi.org/10.1021/acs.inorgchem.1c00444.
- [56] P.D. Mestizo, D.M. Narváez, J.A. Pinzón-Ulloa, D.T. Di Bello, S. Franco-Ulloa, M. A. Macías, H. Groot, G.P. Miscione, L. Suescun, J.J. Hurtado, Novel complexes with ONNO Tetradentate Coumarin Schiff-Base donor ligands: X-ray structures, DFT calculations, molecular dynamics and potential anticarcinogenic activity, Biometals 34 (2021) 119–140, https://doi.org/10.1007/s10534-020-00268-8.
- [57] G. Darcis, G. Van Der Auwera, J. Giot, M. Hayette, F. Tassin, J.A. Estrada, L. Cnops, M. Moutschen, L. De Leval, P. Leonard, Recurrence of visceral and muco-cutaneous leishmaniasis in a patient under immunosuppressive therapy, BMC Infect. Dis. 17 (2017) 2-4, https://doi.org/10.1186/s12879-017-2571-x.
- [58] D. Belkhir-Talbi, M. Makhloufi-Chebli, S. Terrachet-Bouaziz, D. Hikem-Oukacha, N. Ghemmit, L. Ismaili, et al., Synthesis, characterization, theoretical studies, ADMET and drug-likeness analysis: electrochemical and biological activities of metal complexes of 3-(2-Hydroxybenzoyl)-2h-Chromen-2-one, J. Mol. Struct. 1179 (2019) 495–505, https://doi.org/10.1016/j.molstruc.2018.11.035.
- [59] V. Kaplum, J. Cogo, D. Sangi, T. Ueda-Nakamura, A. Corrêa, C. Nakamura, In vitro and in vivo activities of 2,3-diarylsubstituted quinoxaline derivatives against Leishmania amazonensis, Antimicrob. Agents Chemother. 60 (2016) 3433–3444, https://doi.org/10.1128/AAC.02582-15.
- [60] C.L.A. Passos, R. Rodriguez, C. Ferreira, D.C. Soares, G.V. Somner, L. Hamerski, C. Pinto, C.M. Resende, E.M. Saraiva, Anti-Leishmania amazonensis activity of Serjania lethalis A. St.-Hil, Parasitol. Int. 66 (2017) 940–947, https://doi.org/ 10.1016/j.parint.2016.10.01.

- [61] P. Deolindo, A.S. Teixeira-Ferreira, R.A. DaMatta, E.W. Alves, L-amino acid oxidase activity present in fractions of Bothrops jararaca venom is responsible for the induction of programmed cell death in *Trypanosoma cruzi*, Toxicon 56 (2010) 944–955, https://doi.org/10.1016/j.toxicon.2010.06.019.
- [62] S.L. Calixto, N. Glanzmann, M.M.X. Silveira, J.T. Granato, K.K.G. Scopel, T. T. Aguiar, R.A. DaMatta, G.C. Macedo, A.D. Silva, E.S. Coimbra, Novel organic salts based on quinoline derivatives: the *in vitro* activity trigger apoptosis inhibiting autophagy in *Leishmania* spp, Chem. Biol. Interact. 293 (2018) 141–151, https://doi.org/10.1016/j.cbi.2018.08.003.
- [63] S. Bigyan, X. Liuxing, Y. Fen, W. Wei, Z. Quanming, X. Menghua, Z. Shizhe, L. Wanting, J. Yan, P. Laxman, S. Jun, X. Qicai, G. Liqian, D. Wenbin, Recent advance on PTP1B inhibitors and their biomedical applications, Eur. J. Med. Chem. 199 (2020), 112376, https://doi.org/10.1016/j.ejmech.2020.112376.
- [64] T. Kostrzewa, J. Jonczyk, J. Drzezdzon, D. Jacewicz, M. Górska-Ponikowska, M. Kołaczkowski, A. Kuban-Jankowska, Synthesis, in vitro, and computational studies of PTP1B phosphatase inhibitors based on Oxovanadium(IV) and Dioxovanadium(V) complexes, Int. J. Mol. Sci. 23 (2022) 7034, https://doi.org/ 10.3390/ijms23137034.
- [65] C. Yuan, L. Lu, Z. Liu, M. Guo, S. Xing, X. Fu, M. Zhu, Synthesis, characterization, and protein tyrosine phosphatases inhibition activities of oxovanadium(IV) complexes with Schiff base and polypyridyl derivatives, J. Inorg. Biochem. 104 (2010) 978–986, https://doi.org/10.1016/j.jinorgbio.2010.05.003.
- [66] L. Ma, L. Lu, M. Zhu, Q. Wang, F. Gao, C. Yuan, Y. Wu, S. Xing, X. Fu, Y. Mei, X. Gao, Dinuclear copper complexes of organic claw: potent inhibition of protein tyrosine phosphatases, J. Inorg. Biochem. 105 (2011) 1138–1147, https://doi.org/10.1016/j.jinorgbio.2011.05.015.